ORIGINAL ARTICLE

Molecular Genetics & Genomic Medicine
Open Access
WILEY

Systematic analysis of a mitochondrial disease-causing *ND6* mutation in mitochondrial deficiency

Deyu Chen[1] | Qiongya Zhao[2] ![ORCID] | Jingting Xiong[3] | Xiaoting Lou[1] | Qinxia Han[1] | Xiujuan Wei[1] | Jie Xie[1] | Xueyun Li[1] | Huaibin Zhou[1] | Lijun Shen[1] | Yanling Yang[4] | Hezhi Fang[1] | Jianxin Lyu[1,2] ![ORCID]

[1]Key Laboratory of Laboratory Medicine, Ministry of Education, Zhejiang Provincial Key Laboratory of Medical Genetics, College of Laboratory Medicine and Life sciences, Wenzhou Medical University, Wenzhou, China

[2]Zhejiang Provincial People's Hospital, Affiliated People's Hospital of Hangzhou Medical College, College of Laboratory Medicine, Hangzhou Medical College, Hangzhou, China

[3]Department of Laboratory Medicine, Liyuan Hospital, Tongji Medical College, Huazhong University of Science and Technology, Wuhan, China

[4]Department of Pediatrics, Peking University First Hospital, Peking University, Beijing, China

Correspondence
Yanling Yang, Department of Pediatrics, Peking University First Hospital, Peking University, Beijing, China.
Email: organic.acid@126.com

Hezhi Fang, Key Laboratory of Laboratory Medicine, Ministry of Education, Zhejiang Provincial Key Laboratory of Medical Genetics, College of Laboratory Medicine and Life sciences, Wenzhou Medical University, Wenzhou, Zhejiang, China.
Email: FangH@wmu.edu.cn

Jianxin Lyu, Key Laboratory of Laboratory Medicine, Ministry of Education, Zhejiang Provincial Key Laboratory of Medical Genetics, College of Laboratory Medicine and Life sciences, Wenzhou Medical University, Wenzhou, Zhejiang, China.
Zhejiang Provincial People's Hospital, Affiliated People's Hospital of Hangzhou Medical College, College of Laboratory Medicine, Hangzhou Medical College, Hangzhou, Zhejiang, China.
Email: jxlu313@163.com

Funding information
National Natural Science Foundation of China, Grant/Award Number: 81830071 and 81741061; Zhejiang Provincial Natural

Abstract

Background: The m.14487T>C mutation is recognized as a diagnostic mutation of mitochondrial disease during the past 16 years, emerging evidence suggests that mutant loads of m.14487T>C and disease phenotype are not closely correlated.

Methods: Immortalized lymphocytes were generated by coculturing the Epstein–Barr virus and lymphocytes from m.14487T>C carrier Chinese patient with Leigh syndrome. Fifteen cytoplasmic hybrid (cybrid) cell lines were generated by fusing mtDNA lacking 143B cells with platelets donated by patients. Mitochondrial function was systematically analyzed at transcriptomic, metabolomic, and biochemical levels.

Results: Unlike previous reports, we found that the assembly of mitochondrial respiratory chain complexes, mitochondrial respiration, and mitochondrial OXPHOS function was barely affected in cybrid cells carrying homoplastic m.14487T>C mutation. Mitochondrial dysfunction associated transcriptomic and metabolomic reprogramming were not detected in cybrid carrying homoplastic m.14487T>C. However, we found that mitochondrial function was impaired in patient-derived immortalized lymphocytes.

Conclusion: Our data revealed that m.14487T>C mutation is insufficient to cause mitochondrial deficiency; additional modifier genes may be involved in m.14487T>C-associated mitochondrial disease. Our results further demonstrated that a caution should be taken by solely use of m.14487T>C mutation for molecular diagnosis of mitochondrial disease.

Deyu Chen, Qiongya Zhao and Jingting Xiong are contributed equally to this work.

1 | INTRODUCTION

Mitochondrial disease is a subset of genetic disorders characterized by insufficient production of mitochondrial energy, namely adenosine triphosphate (ATP). The oxidative phosphorylation system (OXPHOS) plays a central role in ATP generation by converting carbon sources, such as glucose, to H_2O and CO_2 during electron transfer, and in the phosphorylation of ADP via ATP synthase. Since 2019, over 290 genes associated with OXPHOS abnormalities have been identified, of which 50 genes encode structural subunits of the OXPHOS (Alston et al., 2018; Frazier, Thorburn, & Compton, 2017; Pacheu-Grau et al., 2018). As the OXPHOS structural subunits can be encoded in either the nuclear DNA (nDNA) or the mitochondrial DNA (mtDNA), mitochondrial disease can show both maternal and Mendelian inheritance patterns.

The OXPHOS comprises five complexes and each complex has a considerable number of structural subunits. There are 45 structural subunits for respiratory chain complex (RCC) I, 4 for RCC II, 11 for RCC III, 14 for RCC IV, and 14 for ATP synthase (Balsa et al., 2012; Signes & Fernandez-Vizarra, 2018). In human cells, each mitochondrion has its own genetic material and accounts for the encoding of 13 structural subunits for OXPHOS complexes, excluding RCC II. Before the era of next-generation sequencing (NGS), the in-depth screening of mitochondrial disease-associated nDNA mutations was impossible. However, since mtDNA has a length of 16,569 bp and contains only 37 genes, the detection of mitochondrial disease-associated mtDNA mutations was relatively easy using direct Sanger sequencing of the entire mitochondrial genome in energy-dependent tissues, followed by radiolabeling based on mutant load analysis. In 1988, the first mitochondrial disease-causing mutation, the m.11778G>A point mutation in *MT-ND4*, was identified in a patient with Leber's hereditary optic neuropathy (LHON) (Wallace et al., 1988). However, recently, few mtDNA mutations have been reported, partly due to the fact that the mitochondrial disease-associated mtDNA mutation spectrum has been well characterized (Frazier et al., 2017).

Precision diagnosis and clinical consultation for mtDNA disease is somewhat uncertain, specifically in patients carrying novel mtDNA mutations. One of the major reasons is that most mtDNA mutations are heteroplasmic, a unique feature of mtDNA mutations in which the mutation occupies some, but not all, of the hundreds of mtDNA copies that one cell can contain. The clinical symptoms appear only when the rate of mtDNA mutation (heteroplasmy) reaches a specific "threshold" level (Zinchuk, Wu, & Grossenbacher-Zinchuk, 2013). However, determination of this mtDNA mutation threshold is difficult and the mutation may be detected only in certain affected tissues in a small portion of patients. This may limit the diagnosis of mtDNA-associated mitochondrial heart and brain disease and lead to false negative diagnoses if other tissues are tested. Moreover, the lack of functional mtDNA mutation evaluations may lead to false positive diagnoses (Bornstein et al., 2002). Another aspect that hinders precision diagnosis and clinical consultation is that the genotype–phenotype associations of mtDNA disease vary between patients. The clinical severity and subtypes of mitochondrial disease have been associated with the loads of mutant mtDNA. For example, mutant loads of m.3243A>G at 10%–30%, 50%–90%, and 90%–100% manifest as diabetes and autism, encephalomyopathy, and perinatal lethality (Picard et al., 2014), respectively. Nevertheless, there are still many disease phenotypes that cannot be solely explained by mtDNA mutant loads. Modifier factors such as genetic backgrounds and secondary gene mutations may be responsible for the modulation of the clinical expression of mtDNA disease (Guan et al., 2006; Ji et al., 2008; Qu et al., 2009), further complicating this complex disease.

The m.14487T>C mutation at *MT-ND6,* was first described as a causative mutation of Leigh syndrome in children from three different studies (Lebon et al., 2003; Solano et al., 2003; Ugalde et al., 2003). To date, multiple subtypes of mitochondrial disease, such as LHON (Eckenweiler et al., 2015), cardiomyopathy (Dermaut et al., 2010), visual loss (Dermaut et al., 2010), and diabetes (Dermaut et al., 2010), have been found to be associated with m.14487T>C mutation. A functional study using cybrid technology revealed that heteroplasmic *ND6* mutations at 60% caused RCC I defects (Ugalde et al., 2003), while homoplasmic *ND6* mutations led to losses of RCC I-dependent respiration (Solano et al., 2003). This indicates that m.14487T>C is a severe mtDNA mutation. Notably, mutant loads of m.14487T>C and disease phenotype are not closely correlated. Although extremely high mutant loads in patients carrying m.14487T>C were associated with severe mitochondrial disease such as Leigh syndrome (Wang et al., 2009), a few patients carrying nearly homoplasmic m.14487T>C developed mild mitochondrial disease, including hearing loss and LHON (Dermaut et al., 2010). Moreover, 50% heteroplasmic m.14487T>C was shown to cause a dramatic decrease of RCC I activity in patients' muscles (Malfatti et al., 2007), but RCC I activity

was not affected in some patients with 65%–85% heteroplasmic m.14487T>C (Lebon et al., 2003; Leshinsky-Silver et al., 2011; Ugalde et al., 2003). Therefore, the causative role of m.14487T>C mutation in RCC I deficiency requires further interpretation. Here, we generated multiple cybrid cell lines containing either wild-type or homoplasmic mutant m.14487T>C mtDNA and investigated the influence of m.14487T>C on mitochondrial function at the biochemical and multiomics levels. Our findings show that homoplasmic m.14487T>C mutations derived from Chinese patients have minimal impact on the function of the mitochondrial OXPHOS, suggesting that other modifier factors, such as genetic background, may be involved in the regulation of m.14487T>C-associated mitochondrial disease.

2 | MATERIALS AND METHODS

2.1 | Ethical compliance

Informed consent was obtained from all three subjects under protocols approved by the Ethical Committee of the Peking University First Hospital, and the ID of the Ethics Committee is 2017–217.

2.2 | Participants

Blood from three genetically unrelated patients carrying m.14487T>C was used to generate transmitochondrial cell lines (cytoplasmic hybrids, cybrids). All patients were clinically diagnosed with mitochondrial Leigh syndrome via physical examination, magnetic resonance imaging examination, and blood biochemical analysis. The clinical presentation of all three patients is described in Table S1. All experimental methods were carried out according to the approved guidelines of the Peking University First Hospital.

2.3 | Cybrid cells and culture conditions

Transmitochondrial cybrids were obtained by fusion of mtDNA-less ρ0 human osteosarcoma 143B cells with platelets, which were isolated from the blood of patients and their mothers, as described previously (Chomyn et al., 1994). The transformant clones were cultured in high-glucose Dulbecco's modified Eagle's medium (Sigma-Aldrich) containing 10% bovine calf serum (Sigma-Aldrich) at 37°C in a humidified CO_2 incubator. Four clones containing two cybrids cells carrying homoplasmic m.14487T (L) and two cybrids cells carrying homoplasmic m.14487C (H) were selected from each patient for subsequent experiments. Cybrid cells carrying m.3697G>A in MT-ND1 were previously described (Sun, Li,

Qiu, Fang, & Lyu, 2016). Mycoplasma contamination was tested with a MycoAlert PLUS Mycoplasma Detection Kit (Lonza). Mycoplasma contamination was avoided or eliminated by culturing the cybrid cells with medium containing BM-Cyclin, according to the manufacturer's instructions (Roche).

2.4 | Karyotyping

For the cytogenetic analysis of the cybrids, the cells were exposed to colchicines (0.2 µg/ml) for 6 hr at 37℃ and harvested routinely. Metaphases were prepared from the cybrids with a freshly prepared cold fixative solution (3:1 methanol:acetic acid). Chromosome spread preparations were made as previously described(Frydrychova & Marec, 2002). Preparations were stained for 30 min. Images were acquired and analyzed under an Olympus BX41 microscope (Olympus Corporation). Around 20 metaphase cells were captured for analysis for each cell line.

2.5 | Mitochondrial DNA analysis

Genomic DNA was extracted using a sodium dodecyl sulfate (SDS) lysis protocol (Sambrook & and Russell, 2001). The entire mtDNA genome from the patient was Sanger sequenced with 24 previously reported pairs of mtDNA primers (Rieder, Taylor, Tobe, & Nickerson, 1998). A PCR-RFLP method was used to quantify the mutant load of m.14487T>C in clinical samples and cybrid clones. The PCR primer sequences used in this study were as follows: Set 1: forward (m.14232), 5'-AATCATACAAAGCCCCCGCA-3'; reverse (m.14859), 5'-CCAAGGAGTGAGCCGAAGTT-3'; Set 2: forward(m.14082),5'-GCATAATTAAACTTTACTTC-3'; reverse (m.15017), 5'-AGAATATTGAGGCGCCATTG-3. A 628-bp or 937-bp segment of PCR product was subjected to complete digestion with BsaX I (NEB, New England Biolabs) at 37°C. The m.14487C-containing fragment was cut into two smaller fragments of 372 and 256 bp, or 407 and 530 bp, while the m.14487T-containing fragment remained intact. The mutant loads of m.14487T>C in the cybrids during culture were reexamined frequently by PCR-RFLP. Band intensities were quantified by Gel-Pro Analyzer 4.0 (Media Cybernetics, Warrendale, PA, USA). NGS technology was adopted to further confirm the mutant load of m.14487T>C in selected cybrid cells. The sequences of two pairs of long-range PCR primers were as follows: forward_1 (m.807), 5'-ACGGGAAACAGCAGTGATTAAC-3'; reverse_1 (m.9342), 5'-CTAGTATGAGGAGCGTTATGGAGTG-3'; forward_2 (m.8998), 5'-GTACGCCTAACCGCTAA

CATTACT-3'; reverse_2 (m.1163), 5'-GTTTTAAGCTG TGGCTCGTAGTG-3'. A tetra-primer amplification refractory mutation system-quantitative PCR was used to verify the mutant loads of m.3842G>A and m.11363G>A identified by NGS. The sequences of two pairs of PCR primer used for allele-specific quantitative PCR were as follows: forward_1 (m.3822, G allele), 5'-CTGATTACTCCTGCCATCCTG-3'; reverse_1 (m.3997), 5'-TGTTTGTGTATTCGGCTATGAAG-3'; forward_2 (m.3714, A allele), 5'-AGCCCAAACAAT CTCATATGAAG-3'; reverse_2 (m.3867), 5'-GATA AATCATATTATGGCCAAGGTTT-3'; forward_1 (G allele) (m.11208), 5'-TATTCTACACCCTAGTAGGCTC-3';reverse_1(m.11386),5'-AAGAGGTATCTTTACTATA AACGC-3'; forward_2 (m.11339, A allele), 5'-TTAATAT GACTAGCTTACACAAGAA-3'; reverse_2 (m.11478), 5'- CCGCCTAGTTTTAAGAGTACT-3'. Mutation of m.3697G>A was confirmed by Sanger sequencing.

2.6 | Whole exome sequencing

DNA was extracted from EDTA blood samples from each patient and their biological parents (trio) using a QIAamp DNA Mini Kit (QIAGEN) and quantified with the Nanodrop system (Thermo Scientific). Whole exome sequencing of the samples was performed at Eulertechnology, Inc. (Beijing). The pathogenicity of the variants was filtered by the consistency with the recessive model of pathogenesis, allele frequency and effect on protein function (Calvo et al., 2012).

2.7 | Measurement of oxygen consumption

Endogenous oxygen consumption from intact cells was determined using a Clark-type oxygen electrode (Oroboros Instruments), as described previously (Zhou et al., 2018). For measuring oxygen consumption using the XF24 Analyzer (Seahorse Biosciences), 4×10^4 cells were seeded and OCR was assayed in a Seahorse XF-24 extracellular flux analyzer by the sequential addition of 1 mM oligomycin, 1 mM carbonyl cyanide-p-trifluoromethoxyphenylhydrazone, and 1 mM rotenone plus 1 mM antimycin A (Gaude et al., 2018).

2.8 | Mitochondrial isolation and RCC enzyme activity assay

Mitochondria from cultured cells were isolated as previously described with minor modifications (Fernandez-Vizarra et al., 2010). The enzyme activity of RCC I was measured and normalized against citrate synthase as described previously (Birch-Machin & Turnbull, 2001).

2.9 | BN-PAGE, SDS-PAGE, immunoblotting, and antibodies

Proteins from whole cell were extracted with RIPA lysis buffer (Cell Signaling Technology) supplemented with a protease inhibitor cocktail (Sigma-Aldrich). Native mitochondrial membrane proteins were solubilized in digitonin (Sigma-Aldrich) at a ratio of 20-mg wet weight cells/2-mg digitonin or in n-Dodecyl β-D-maltoside (DDM, Sigma-Aldrich) at a ratio of 20-mg wet weight cells/1 mg DDM in 40-μL solubilization buffer [50 mM sodium chloride, 50 mM imidazole, 2 mM 6-aminohexanoic acid, and 1 mM EDTA (all from Sigma-Aldrich), pH 7.0 at 4°C]. The supernatant containing the membrane proteins was retained after centrifugation at $20,000 \times g$ for 30 min. For mitochondrial OXPHOS complex analyses, 60-μg native mitochondrial membrane proteins containing 0.5% Blue G-250 (Sigma-Aldrich) and 5% glycerol were separated by BN-PAGE (3%–11% gel), as previously described (Wittig, Braun, & Schagger, 2006). The proteins separated by BN-PAGE or SDS-PAGE were transferred to 0.22-μm PVDF membranes (Bio-Rad, Hercules, CA, USA) using a semi-dry transfer system (Bio-Rad). The proteins were probed with anti-Grim19 (ab110240; 1:1000), anti-SDHA (ab14715; 1:1000), anti-UQCRC2 (ab14745; 1:1000), anti-ATP synthase subunit-α (ab14748; 1:1000), anti-MTCOI (ab14705; 1:1000), anti-CLPP (ab124822; 1:1000), anti-MFN1 (ab57602; 1:1000), anti-MFN2 (ab56889; 1:1000), anti-OPA1 (ab42364; 1:1000), anti-DRP1 (ab184247; 1:1000), anti-PAPOLG (ab203751; 1:1000), anti-TOMM20 (ab186734; 1:1000, all from Abcam, Cambridge, MA), anti-AFG3L2 (AP13219a; 1:1000, ABGENT, San Diego, USA), anti-TOMM70 (#14528-1-AP; 1:2000), anti-AKT1 (#2938; 1:1000), anti-phospho-AKT Ser473 (#12694; 1:1000), anti-P38 (#8690; 1:1000), anti-phospho-P38 (#4511; 1:1000), anti-SRC (#2109; 1:1000), anti-phospho-SRC (#2105; 1:1000), anti- p44/42 MAPK (Erk1/2) (#9102; 1:1000), anti-phospho-p44/42 MAPK (Erk1/2) (Thr202/Tyr204) (#4370; 1:1000), anti-JNK (#9252; 1:1000), anti-phospho-JNK (#4668; 1:1000), anti-SOD1 (ab16831; 1:1000), anti-SOD2 (sc-133254; 1:1000), anti-Catalase (#14097; 1:1000), anti-Thioredoxin1 (#2429; 1:1000), anti-Peroxiredoxin1 (#8499; 1:1000), anti-TFAM (#8076; 1:1000, all from Cell Signaling Technology), anti-PGC-1 (sc-13067; 1:1000), anti-RXRA (sc-553; 1:1000), anti-HSP60 (sc-376261; 1:2000), anti-GRP75 (sc-133137; 1:1000), and anti-β-actin (sc-47778; 1:5000; all from Santa Cruz Biotechnology, Santa Cruz, CA). Alkaline phosphatase-conjugated anti-mouse IgG (#7056; 1:2000; Cell Signaling Technology) or horseradish peroxidase-conjugated anti-rabbit/mouse IgG (#7074/#7076; 1:2000; Cell Signaling Technology) were used as secondary antibodies. Signals were detected with Clarity Western ECL Substrate (Bio-Rad) or 5-bromo-4-chloro-3′-indolyl

phosphate p-toluidine (20 mg/ml, Thermo Fisher Scientific)/ nitrotetrazolium blue chloride (10 mg/ml, Sigma-Aldrich).

2.10 | ATP, Mitochondrial membrane potential and ROS measurements

ATP, mitochondrial membrane potential and ROS were measured using an ATP measurement kit (Thermo Fisher Scientific), the cationic fluorescent redistribution dye, tetramethylrhodamine methyl ester (TMRM, Thermo Fisher Scientific), the MitoSOX and Carboxy-DCFDA dyes (both from Thermo Fisher Scientific) respectively, as described previously (Fang et al., 2018). The relative level of ATP, mitochondrial membrane potential and ROS was normalized by protein concentration or cell area.

2.11 | Immunofluorescence staining

Cells were cultured on coverslips and fixed with 4% paraformaldehyde/PBS, and then they were incubated overnight with anti-HSP60 (1:300; Santa Cruz Biotechnology) or anti-LC3B (1:250; Cell Signaling Technology) antibodies at 4°C in a darkroom. After washing and incubating with a fluorescently labeled secondary antibody, either IgG-Alexa Fluor 594 or IgG-Alexa Fluor 488 (1:300; Cell Signaling Technology). A final incubation was performed to stain the cells with DAPI (Beyotime)(Zhou et al., 2018). Images were captured using a confocal laser microscope at $600 \times$ magnification (Nikon). Pearson's correlation coefficients were calculated with Image J v2.4.1.7 using 40 cells from 10 images (four cells per image) for each cell line (Zinchuk et al., 2013). Fragmented mitochondria-containing cells were quantitatively defined using Image J, according to published criteria (Wang et al., 2016).

2.12 | Aspartate measurement

The aspartate level was measured using an aspartate assay kit (Abcam) according to the manufacturer's instructions. Fluorescence was record by the Varioskan™ Flash Multimode Reader (excitation/emission: 535/590 nm) (Thermo Fisher Scientific). The relative aspartate level was normalized against cell number.

2.13 | Cell proliferation assay

Cell Counting Kit-8® solution (Dojindo) was used for cell proliferation measurement according to the manufacturer's protocol. Briefly, 4×10^3 cells/100 μL were seeded in 96-well plates and treated with 10 μL of Cell Counting Kit-8® solution. The optical

density of the wells was measured at 450 nm using a Varioskan™ Flash Multimode Reader (Thermo Fisher Scientific).

2.14 | mtDNA content, mtRNA gene expression

Genomic DNA and total RNA were extracted using standard protocols and quantitative real-time PCR was performed with previously reported primers(Fang et al., 2018) on a CFX96 Touch™ Real-Time PCR Detection System (Bio-Rad) using SYBR® Green qPCR Mastermix (Bio-Rad). Both the mtDNA content and the mRNA levels were determined using the $2^{(-\Delta\Delta CT)}$ method, as previously described (Fragouli et al., 2015).

2.15 | Sample preparation and transcriptome analysis

Total RNA was isolated from each cybrid cell ($n = 3$) and then the library construction and sequencing were performed by Novogene, as described previously (Fang et al., 2018). The number of reads of mapped gene was obtained by the standard pipeline, differential expression analysis was performed using the DESeq2 R package. Genes featured an adjusted $p < .05$ were regarded as DEGs. To identify the DEGs between the cybrids carrying m.14487T>C and the control cybrids, we combined two L cybrid cells as the wild group, and two H cybrid cells as the mutant group. Heatmaps were drawn using the R package pheatmap.

2.16 | Sample preparation and metabolomic profiling

Cells ($n = 6$ for each cybrid) were plated in high-glucose Dulbecco's modified Eagle's medium. After 48 hr, the cells were collected and snap frozen in liquid nitrogen. Samples were sent to Metabolon, Inc. for metabolomic profiling. Principal component analysis was used to display the overall differences. Differences between groups in the abundance of metabolites were assessed by Welch's two-sample t test for the multivariate model analysis. Differences were considered statistically significant at $p < .05$.

2.17 | Statistical analysis

All experiments were performed in triplicate and were performed independently at least three times for each cybrid cell. Data are presented as the mean $\pm$ standard error of the mean. Significance was estimated using either an independent Student's t test (number of comparations = 1) or a One-Way ANOVA (number of comparations ≥2) for cybrid data, except

for the NGS data and metabolomics data. For m.14487T>C, a significant difference between mutant cybrids and wild-type cybrids was accepted only when all comparisons in the One-Way ANOVA met the criterion of $p < .05$. For m.3697G>A, the null hypothesis was rejected when $p < .05$.

2.18 | Accession numbers

The data that support the findings of this study are available on request from the corresponding author. All data including WES data, transcriptome data are deposited in the GEO database (accession number: GSE131741).

3 | RESULTS

3.1 | Validation of m.14487T>C cybrid cell model

To generate m.14487T>C cybrid cells, three unrelated patients carrying m.14487T>C but no other disease-causing

mtDNA mutations were recruited. Mutant load analysis using polymerase chain reaction restriction fragment length polymorphism (PCR-RFLP) showed 85%, 95%, and 100% m.14487C in the blood of patient 1, patient 2, and patient 3, respectively, whereas m.14487C was absent in the blood of all maternal subjects (Figure 1a–c). In family 2, homoplasmic m.14487C was detected in the buccal mucosa of the patient and no such mutation was detected in his mother (Figure 1b). Mutation detection in other tissues was not performed but both clinical presentation (Table S1) and genetic analysis (Figure 1a–c) indicated the onset of m.14487T>C-related mitochondrial disease, according to published reports (Eckenweiler et al., 2015; Lebon et al., 2003; Leshinsky-Silver et al., 2011; Solano et al., 2003; Ugalde et al., 2003; Wang et al., 2009). Decreased cellular respiration (Figure 1d) and mitochondrial RCC assembly (Figure 1e,f) in immortalized lymphocytes from two patients carrying m.14487T>C were confirmed when compared with control lymphocytes. These preliminary results agreed with previously published reports that m.14487T>C mutation contributes to mitochondrial abnormality. To verify the effects of the mtDNA m.14487T>C mutation on mitochondrial function, we established a study
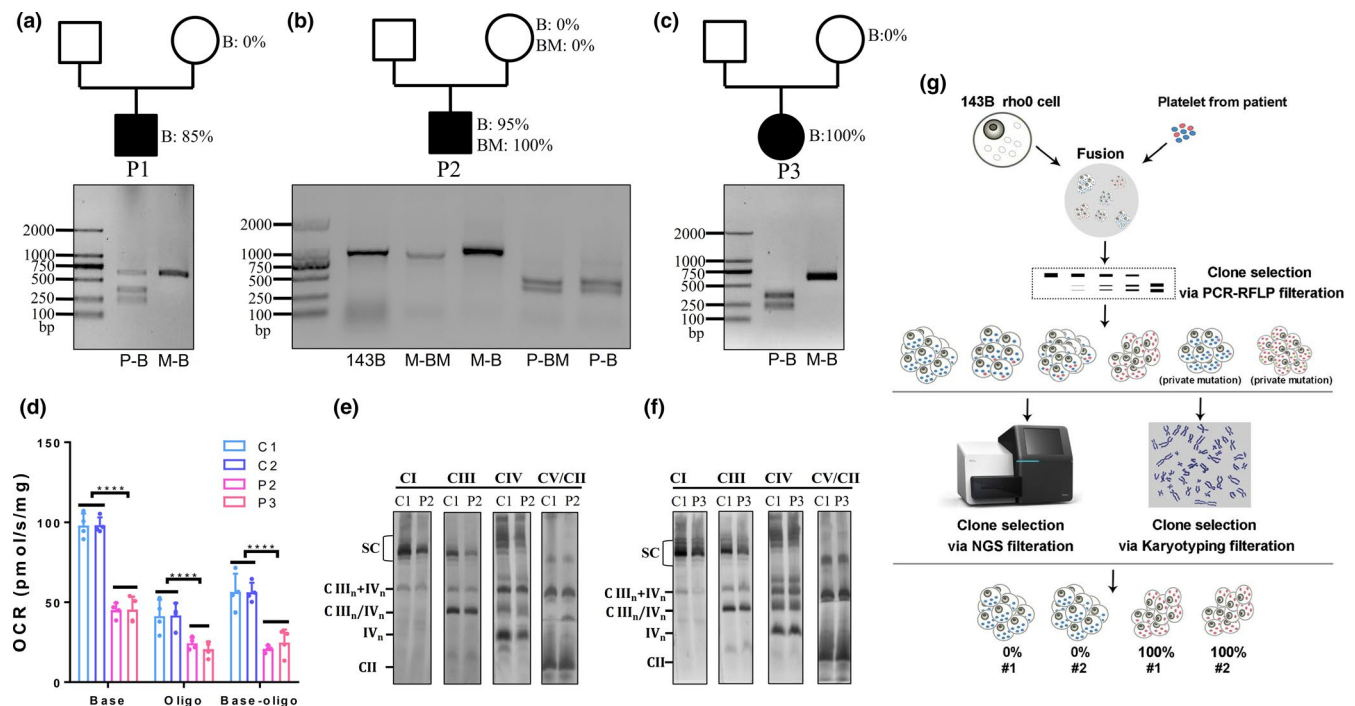

FIGURE 1 Construction of m.14487T>C cybrid model. (a–c) Three family pedigrees are shown as P1 (a), P2 (b), and P3 (c). Mutant load analysis using polymerase chain reaction restriction fragment length polymorphism showed the mutant percentage of m.14487C in the blood and buccal mucosa (P2) (b) from patient 1 (a), patient 2 (b), and patient 3 (c) and their maternal subjects. B: blood; BM: buccal mucosa. (d) Oxygen consumption rate (OCR) in lymphocytes obtained from patient 2, patient 3, and two healthy controls. Base: basal mitochondrial respiration; oligo: uncoupled mitochondrial respiration, measured in the presence of oligomycin (2 µg/mL); Basal-oligomycin: ATP-linked mitochondrial respiration, calculated by subtracting OCR in the presence of oligomycin from basal OCR. (e-f) Respiratory chain supercomplexes in lymphocytes obtained from patient 2 (e), patient 3 (f), and a healthy control. Digitonin-solubilized cell lysates were analyzed by Blue Native PAGE/immunoblotting. Complexes I–V were probed with antibodies against Grim19, SDHA, UQCRC2, COXI, and ATP5a, respectively. (g) A strict standard to select cybrid clones with or without m.14487T>C mutations. Different colors represent different mutations in the mtDNA. Blue: m.14487T; red: m.14487C; purple and green: private mutations. All experiments were performed independently at least thrice. Data are presented as means ± *SEM*. ***$p < .001$

model by generating cybrids with and without m.14487T>C mutation, following a strict standard (Figure 1g). Generally, for each patient, cybrids carrying homoplasmic m.14487T or m.14487C were selected from dozens of clones using PCR-RFLP (Figure S1a). Next, NGS of the mitochondrial genome was performed in all 12 cybrids (four per patient) for the following purposes: a. to ensure the selection of cybrid clones containing homoplasmic m.14487T or m.14487C, otherwise, candidate clones with homoplasmic m.14487T or m.14487C indicated by PCR-RFLP were recruited until NGS verified that homoplasmic m.14487T or m.14487C cybrids had been selected; and b. to avoid the use of cybrids with somatic mtDNA mutations or clonal expansions of mtDNA mutations other than m.14487T>C during cybrid clone selection. As shown in Tables S2 and S3, homoplasmic m.14487T or m.14487C was confirmed and no other private mtDNA mutations were detected in the cybrids from patient 1 or 2. Unexpectedly, we did find a private m.3842G>A (53.78%) mutation with a considerable mutant load in one cybrid from patient 3 (L3-#1) (Table S4), which was further confirmed by allele-specific quantitative PCR (74%). Bioinformatics analysis showed that a codon for an evolutionarily conserved amino acid tryptophan (W) was replaced with a terminator codon in cells with m.3842G>A mutations (Figure S1b). L3-#1 was therefore not used in this study. Furthermore, another private mtDNA mutation, m.11363G>A, was detected in H3-#1 with a low mutant load (16.7%) (Table S4) and confirmed by allele-specific quantitative PCR (7%). Although bioinformatics analysis indicated that an evolutionarily conserved amino acid Alanine (A) was replaced by threonine (T) at position 202 in the cell with m.11363G>A mutation (Figure S1c), we included this cybrid for further study (with caution), while the mutant load was low. Moreover, karyotyping was performed in all 12 cybrids and no significantly differences were observed between the cybrids from any patients (Table S5). Lastly, experimental conditions throughout this work were quality controlled using cybrids with homoplasmic m.3697G>A mutations, a mutation that has long been associated with RCC I deficiencies and mitochondrial disease such as Leigh Syndrome, mitochondrial encephalomyopathy, lactic acidosis, and stroke-like episodes (Kirby et al., 2004; Negishi et al., 2014).

3.2 | Homoplasmic m.14487T>C mutations do not affect mitochondrial RCC I or supercomplex assembly in cybrid cells

The m.14487T>C mutation was shown to impaired RCC I assembly in both cybrid cells and tissues biopsies (Ugalde et al., 2003). To verify the causative role of m.14487T>C mutation, we determined the RCC level in cybrid cells derived from three patients carrying homoplasmic m.14487T>C

mutations. Unexpectedly, the steady-state levels of RCC I, RCC III, RCC IV, and mitochondrial complex V in the m.14487C cybrid cells were similar to those in paired control m.14487T cybrid cells (Figure 2a–c). As one study had claimed that only mitochondrial supercomplexes contain assembled and activated holo-RCC I in 143B cells (Moreno-Lastres et al., 2012), we asked if the super assembly of RCC I + III or RCC I + III+IV, was affected by m.14487T>C. However, the steady-state levels of these mitochondrial supercomplexes were not changed by m.14487T>C mutation in the cybrids derived from patient 1 (Figure 2d), patient 2 (Figure 2e), or patient 3 (Figure 2f). Notably, by adopting the same Blue Native polyacrylamide gel electrophoresis (BN-PAGE)/immunoblot technology conditions, decreased RCC I-containing supercomplexes were found in cybrid cells with homoplasmic m.3697G>A mutations (Figure S2), suggesting that the conditions used in this study were reliable. Taken together, these findings provide biochemical evidence indicating that m.14487T>C mutations may not be enough to impair RCC and mitochondrial supercomplex assembly in our cybrid models. Therefore, it is not surprising that both the mtDNA-lacking 143B cells and the cybrids carrying m.3697A cannot grow well in galactose medium when compared with wild-type 143B cells and cybrids carrying m.3697G, respectively (Figure 2g,h), while the growth capacity of cybrids carrying m.14487C in galactose is comparable to that of cybrids carrying m.14487T (Figure 2i–k).

3.3 | The homoplasmic m.14487T>C mutation does not affect mitochondrial function in cybrid cells

Since some mtDNA mutations impair mitochondrial function without changing RCC assembly (Malfatti et al., 2007), we then asked if m.14487T>C mutation impaired mitochondrial respiration without affecting RCC I assembly in our cybrid models. Unexpectedly, we did not see significant alternations in endogenous mitochondrial respiration, ATP-linked mitochondrial respiration (basal respiration and oligomycin-resistant respiration), or respiratory control ratios (defined by basal respiration/oligomycin-resistant respiration) in mutant cybrids compared with wild-type cybrids (Figure 3a–c). To validate the effect of m.14487T>C mutation on mitochondrial respiration, we performed mitochondrial respiration assays in cybrid cells using Seahorse XF Analyzers, another well-established platform for measuring the oxygen consumption rate (OCR) in live cells. Consistently, we did not see any change of OCR in mutant cybrids compared with paired wild-type cybrids derived from patient 1 (Figure 3d,e); however, homoplasmic m.3697G>A mutations did considerably impair OCR, especially ATP-linked OCR (Figure 3f,g), indicating that the OCR measurement platforms we used in
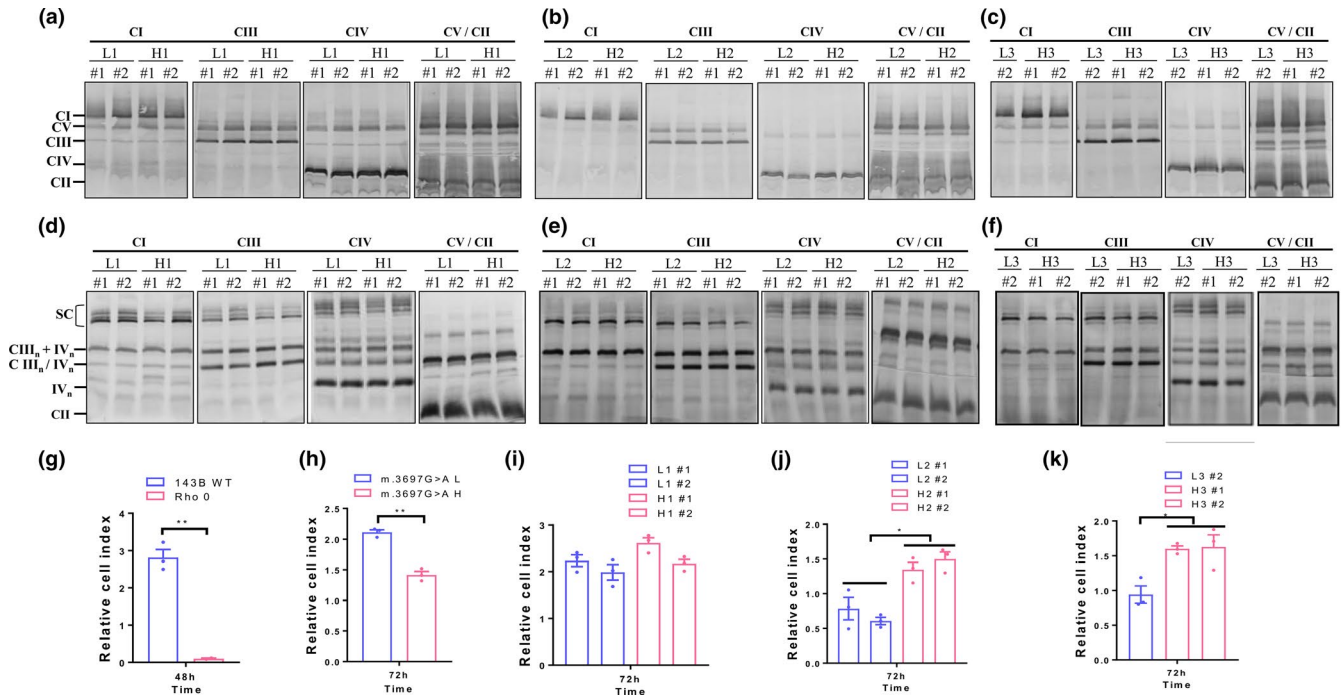
FIGURE 2 Homoplasmic m.14487T>C mutations do not affect mitochondrial RCC I or supercomplex assembly in cybrid cells. (a–c) Respiratory chain single complexes in cybrids containing m.14487T>C mutations from patient 1 (a), patient 2 (b), and patient 3 (c) and their paired control cybrids. (d–f) Respiratory chain supercomplexes in cybrids containing m.14487T>C mutations from patient 1 (d), patient 2 (e), and patient 3 (f) and their paired control cybrids. In (a–f), Digitonin-solubilized cell lysates were analyzed by Blue Native PAGE/immunoblotting. Complexes I–V were probed with antibodies against Grim19, SDHA, UQCRC2, COXI, and ATP5a, respectively. SC: supercomplex. (g–h) Cell proliferation showing that both mtDNA-lacking 143B cells (g) and cybrids carrying m.3697A (h) did not grow well in galactose medium when compared with wild-type 143B cells and cybrids carrying m.3697G, respectively. (i–k) Cell proliferation showing the growth capacity of cybrids containing m.14487T>C mutations from patient 1 (i), patient 2 (j), and patient 3 (k) are comparable with the paired control. All experiments were performed independently at least thrice. Data are presented as means ± *SEM*. *$p < .05$, **$p < .01$, ***$p < .001$, ****$p < .0001$

this study were reliable. Moreover, we failed to detect any RCC I deficiencies in the mutant cybrids when checking the enzyme activity of RCC I (Figure 3h). Similarly, mitochondrial membrane potential, which is closely associated with the function of RCCs, was not altered in mutant cybrids compared with wild-type cybrids (Figure 3i–k). Additionally, cellular ATP levels were similar between mutant and wild-type cybrids (Figure 3l–n), whereas ATP levels were 50% lower in cybrids containing homoplasmic m.3697G>A mutations than in their paired control cybrids (Figure 3o), further demonstrating that a m.14487T>C mutation has a minimal effect on mitochondrial function.

3.4 | Mitochondrial quality control systems were not affected by m.14487T>C mutation

An impaired mitochondrial OXPHOS may lead to the overactivation of mitochondrial quality-control (MQC) systems at the molecular or organelle level to compensate for and restore mitochondrial function (Moehle, Shen, & Dillin, 2019; Zinchuk et al., 2013). Therefore, it would be informative if MQC features were tested in wild-type and

mutant cyprids. Given that molecular MQC is regarded as the first line of defense in this process, we first determined the levels of molecular MQC marker proteins in m.14487T/C and m.3697G>A cybrids. As shown in Figure 4a, red panel, overactivation of molecular MQC was found in m.3697A cybrids but not in m.14487C cybrids, when compared with their paired control cybrids. Next, we asked whether MQC at the organelle level was altered in mutant cybrids. Our results revealed that the expression levels of fission and fusion marker proteins, the long and short forms of OPA1, MFN1/2, and DRP1, were similar in both m.14487C- and m.3697A-containing cybrids, when compared with their paired control cybrids (Figure 4a, blue panel). Furthermore, the percentages of tubular/fragmented mitochondria were similar between mutant (m.14487T>C or m.3697G>A) and control cybrids (Figure 4b-e). This suggests that mitochondrial fission and fusion may not be affected by m.14487T>C or m.3697G>A mutation. In addition, we found that the colocalization coefficient of LC3B and mitochondria was not affected in cybrids with m.14487T>C or m.3697G>A mutations (Figure 4f–i). In addition, mitochondria mass was similarly unaffected by m.14487T>C (Figure 4j
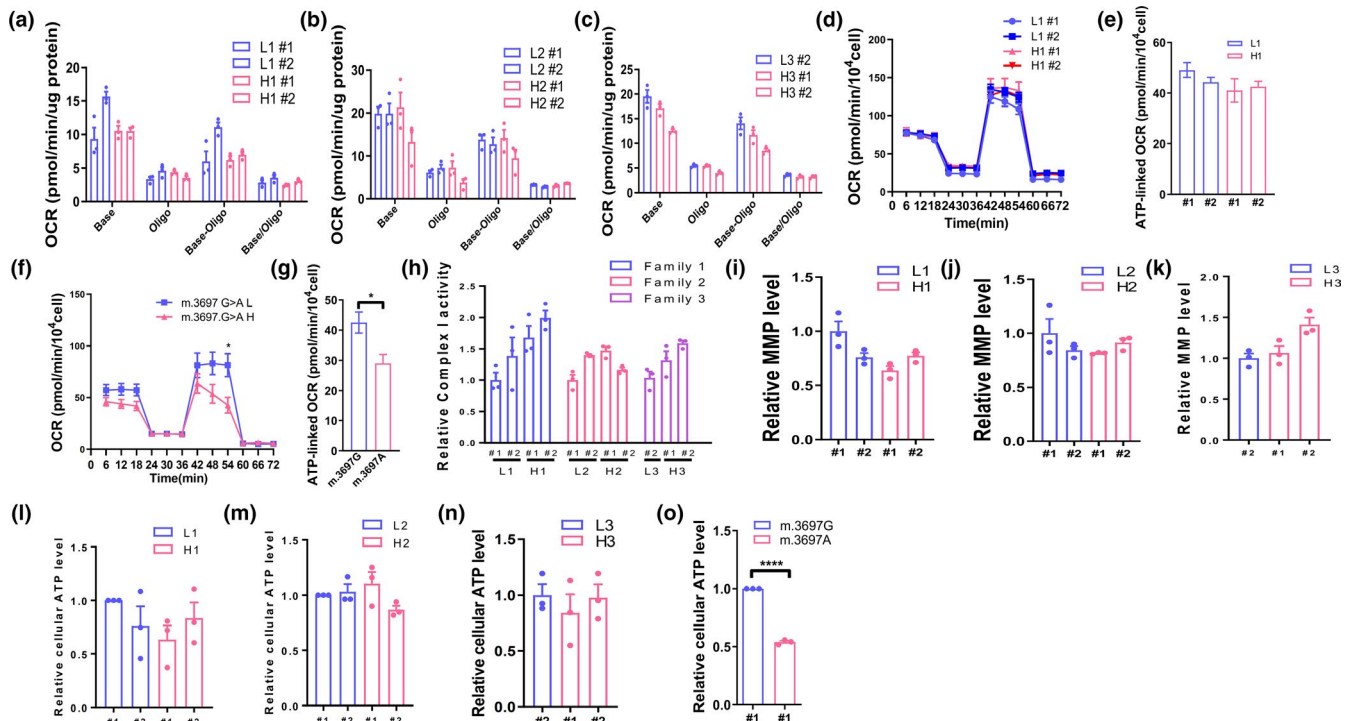
FIGURE 3 The homoplasmic m.14487T>C mutation does not affect mitochondrial function in cybrid cells. (a–c) Oxygen consumption rates (OCRs) in cybrids containing m.14487T>C mutations from patient 1 (a), patient 2 (b), and patient 3 (c) and their paired control cybrids. Base: basal mitochondrial respiration; oligo: uncoupled mitochondrial respiration, measured in the presence of oligomycin (2 μg/mL); Basal-oligomycin: ATP-linked mitochondrial respiration, calculated by subtracting OCR in the presence of oligomycin from basal OCR. Basal/oligomycin: respiratory control ratio, calculated by dividing OCR in the presence of oligomycin by basal OCR. (d,f) Mitochondrial OCR was determined in cybrids from patient 1 containing m.14487T>C mutations (d) or m.3697G>A (f) mutations, and their paired control cybrids ($n = 5$). (e, g) The ATP-linked OCR was calculated by subtracting average OCR in the presence of oligomycin from basal OCR cybrids from patient 1 containing m.14487T>C mutations (e) or m.3697G>A (g) mutations, and their paired control cybrids ($n = 5$). (h) Relative mitochondrial respiratory chain complex activities measured for complex I in cybrids containing m.14487T>C and their paired control cybrids. Respiratory chain complex activities were normalized against citrate synthase activity. (i–k) Relative mitochondrial membrane potential (MMP) in cybrids containing m.14487T>C mutations from patient 1 (i), patient 2 (j), and patient 3 (k) and their paired control cybrids. MMP was normalized against protein concentration. (l–o) Relative ATP content in cybrids containing m.14487T>C mutations from patient 1 (l), patient 2 (m), and patient 3 (n) or m.3697G>A (o) mutations and their paired control cybrids. ATP content was normalized against protein concentration. All experiments were performed independently at least thrice. Data are presented as means ± *SEM*. **$p < .01$, ***$p < .001$

and k) or m.3697G>A (Figure 4j). Our findings suggest that mitophagy was not activated by m.14487T>C or m.3697G>A mutation in cybrid cells. Collectively, our data demonstrate that MQC machineries were partially activated in cybrids containing m.3697G>A but not in cybrids containing m.14487C, which may lead us to believe that mitochondrial function was minimally affect by m.14487T>C mutation.

3.5 | Homoplasmic m.14487T>C mutation does not change ROS-mediated mitochondrial retrograde signaling

Increased reactive oxygen species (ROS) production has been found in cybrid cells with European m.14487T>C (Gonzalo et al., 2005). However, ROS generation, as

determined using either the mitochondrial ROS probe MitoSOX (Figure 5a–c) or the cellular ROS probe carboxy-DCFDA (Figure 5d–f), was not affected by m.14487T>C mutation in this study. However, m.3697A-containing cybrids generated more cellular ROS than m.3697G-containing cybrids (Figure 5g). As antioxidant systems may compensate for and alleviate the oxidative stress caused by mitochondrial abnormality, we determined the levels of antioxidant enzymes in all cybrid cells. As shown in Figure 5h, neither the mitochondrial nor the cellular antioxidant activities differed between the cybrids containing m.14487T>C or m.3697G>A mutations and their paired control cybrids. This suggests that mitochondrial oxidative stress was not altered in cybrids with m.14487T>C mutations, probably due to the fact that mitochondrial function is minimally affected by Chinese m.14487T>C mutations. Consistently, the analysis of five classic ROS-activated
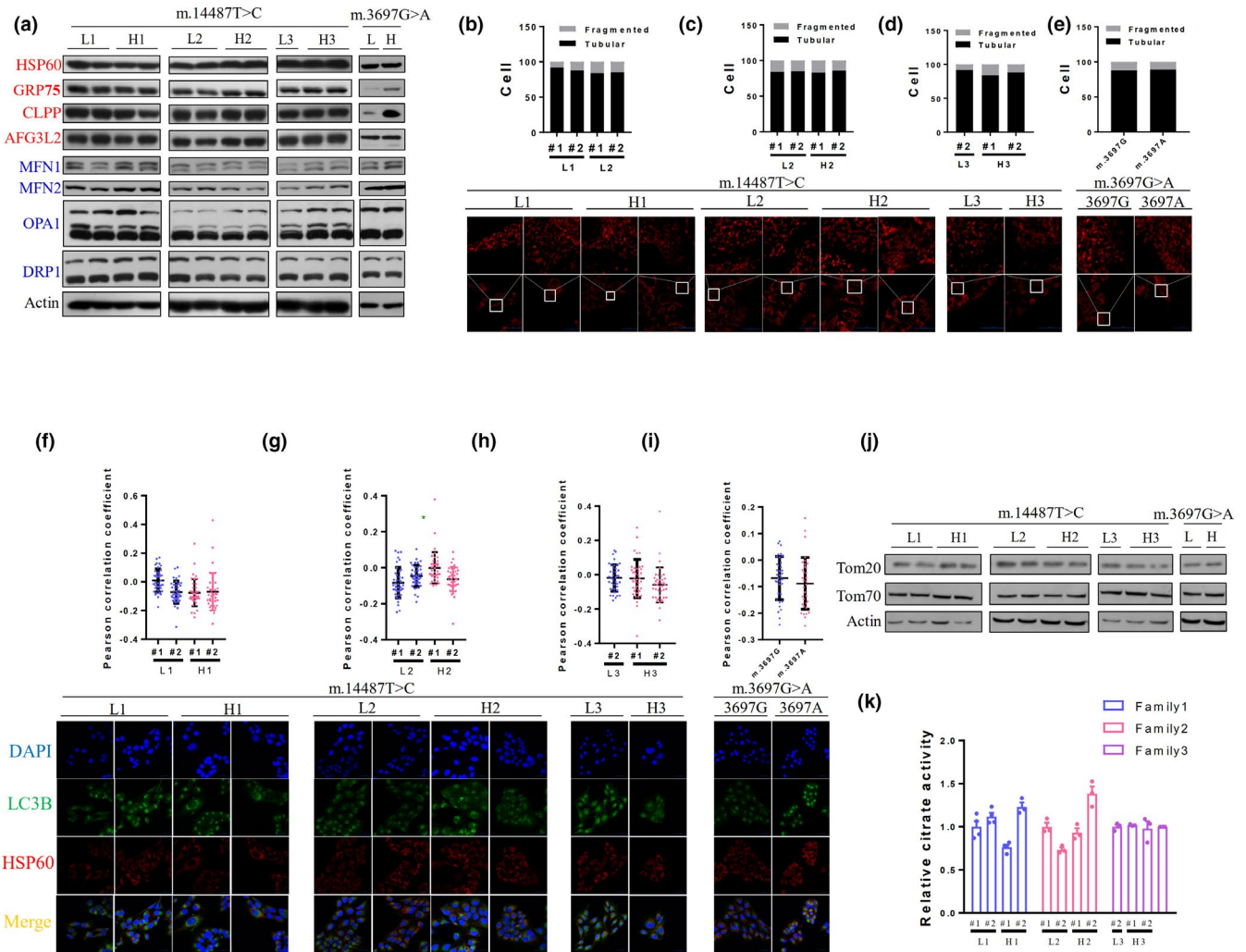
FIGURE 4 Mitochondrial quality control systems were not affected by m.14487T>C mutations. (a) Analysis of mitochondrial quality control (MQC) systems in all cybrid cells. The red panel shows the molecular MQC systems, and the blue panel shows MQC at the organelle level. All cell lysates were analyzed by western blot with antibodies against Hsp60, GRP75, CLPP, AFG3L2, MFN1, MFN2, OPA1, and DRP1. Actin was used as the internal control. (b–d) Stacked bar plot showing the percentages of cybrid cells with or without m.14487T>C mutations from patient 1 (b), patient 2 (c), and patient 3 (d) with fragmented mitochondria ($n = 100$). Images show the mitochondrial morphology in mutant cybrids and paired control cybrid cells from patient 1 (b), patient 2 (c), and patient 3 (d). All cybrid cells were probed with HSP60 (red). (e) Stacked bar plot showing the percentages of cybrid cells with or without m.3697G>A mutations with fragmented mitochondria ($n = 100$). Images show the mitochondrial morphology in cybrid cells with or without m.3697G>A mutations. (f–h) Scatter plot showing the Pearson's correlation coefficients of LC3B (green) and HSP60 (red) colocalization in cybrids with or without m.14487T>C from patient 1 (f), patient 2 (g), and patient 3 (h). Colocalization degree: extremely weak, $-1.0 \sim -0.27$; very weak, $-0.26 \sim -0.09$; moderate, $-0.1 \sim 0.48$; strong, $0.49 \sim 0.84$; and very strong, $0.85 \sim 1.0$. Images show the colocalization of endogenous LC3B and mitochondria in cybrids with or without m.14487T>C from patient 1 (f), patient 2 (g), and patient 3 (h). All cybrids were probed with LC3B (green) and HSP60 (red) antibodies; nuclei were stained with DAPI (blue). (i) Scatter plot showing the Pearson's correlation coefficients of LC3B (green) and HSP60 (red) colocalization in cybrids with or without m.3697G>A. Images show the colocalization of endogenous LC3B and mitochondria in cybrids with or without m.3697G>A. (j) Western blotting showing relative amounts of Tomm20 and Tomm70 in whole-cell extracts. (k) Relative mitochondrial citrate synthase activity in cybrids with or without m.14487T>C. Activity was normalized against mitochondrial protein concentration. Images were acquired using a confocal laser scanning microscope; representative images (600×) are shown. Scale bar: 50 μm. All experiments were performed independently at least thrice. Data are presented as means ± *SEM*

mitochondria-to-nucleus retrograde signaling pathways revealed that ROS-responsive mitochondrial signaling was not affected by m.14487T>C mutation, whereas p38, SRC, and JNK were overactivated by m.3697G>A mutation (Figure 5i). Taken together, our findings indicate that

ROS-mediated mitochondria-to-nucleus retrograde signaling pathways were minimally affected by m.14487T>C mutation, further demonstrating that mitochondrial function is less affected by Chinese m.14487T>C mutation than its European counterpart.
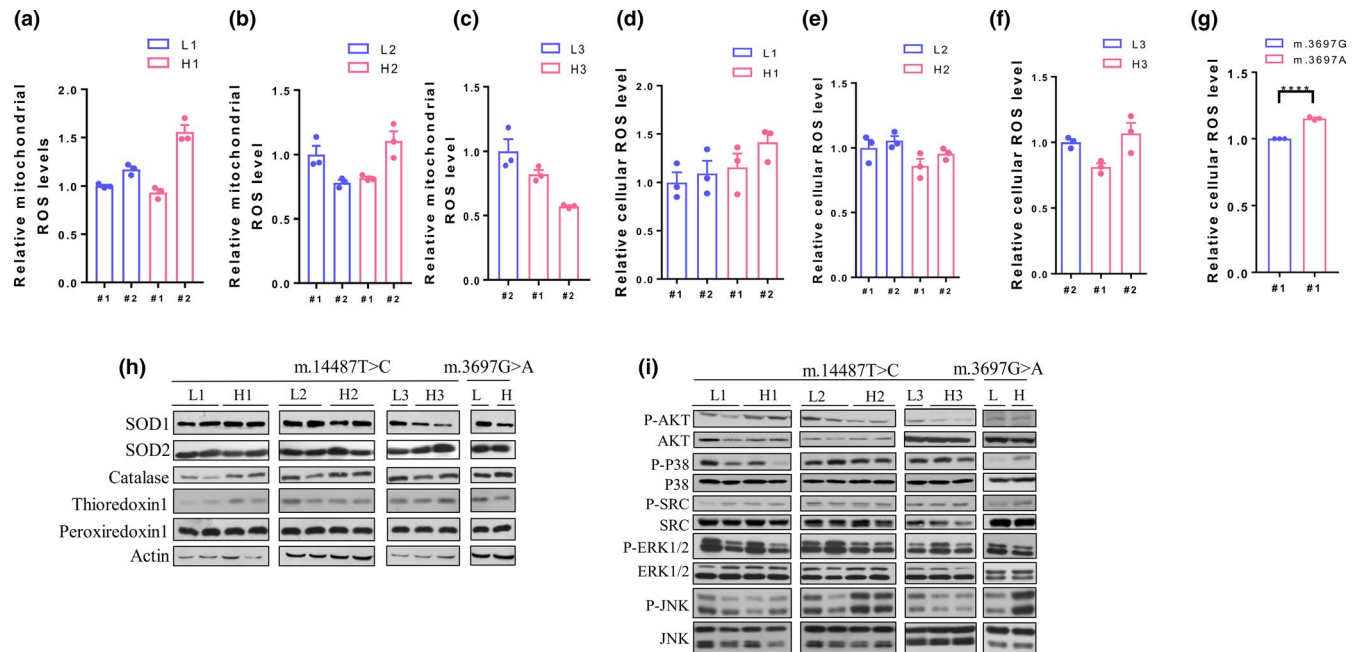
FIGURE 5 Homoplasmic m.14487T>C mutation does not change ROS-mediated mitochondrial retrograde signaling. (a–c) Relative mitochondrial ROS level in cybrids containing m.14487T>C mutations from patient 1(a), patient 2 (b), and patient 3 (c) and their paired control cybrids. (d–f) Relative cellular ROS level in cybrids containing m.14487T>C mutations from patient 1(d), patient 2 (e), and patient 3 (f) and their paired control cybrids. (g) Relative cellular ROS level in cybrids with or without m.3697G>A mutations. (h) Analysis of mitochondrial and cellular antioxidant activity in cybrids with or without m.14487T>C mutations. Cell lysates were analyzed by western blot with antibodies against SOD1, SOD2, Catalase, Thioredoxin1, and Peroxiredoxin1. Actin was used as the internal control. (i) Analysis of mitochondrial-to-nucleus pathways in cybrids with or without m.14487T>C mutations. Cell lysates were analyzed by western blot with antibodies against AKT, p-AKT (Ser473), P38, p-P38, SRC, p-SRC, Erk1/2, p-Erk1/2, JNK, and p-JNK. All experiments were performed independently at least thrice. Data are presented as means ± *SEM*. ****$p < .0001$

3.6 | Transcriptome profiles were minimally affected by homoplasmic m.14487T>C mutations in cybrid cells

Transcriptome profiling is a sensitive strategy used to uncover changes in mitochondrial to nucleus signaling due to minor alternations in mitochondrial OXPHOS function (Picard et al., 2014). We hypothesized that even a minor alternation in OXPHOS function could remold transcriptome profiles in m.14487T>C mutant cybrids, when compared with control cybrids. As shown in Figure S3a–c, the transcriptome profile revealed a considerable number of differentially expressed genes (DEGs) (|FC| >1.5, $P_{adj} < 0.05$) between the m.14487T and m.14487C cybrids, of which 925 upregulated and 531 downregulated genes (Figure S3a), 587 upregulated and 1,266 downregulated genes (Figure S3b), and 1,062 upregulated and 845 downregulated genes (Figure S3c) were identified in m.14487T cybrids as compared with m.14487C cybrids derived from patients 1, 2, and 3, respectively. However, these DEGs were significantly enriched in only 3 and 1 KEGG pathways from patient 1 and patient 3, respectively, and none of them were related to the mitochondrial or mitochondrial retrograde signaling pathways (Table S6). This indicates that most of these DEGs

are biologically nonrelevant. Although the DEGs between the m.14487T and m.14487C cybrids derived from patient 2 were significantly enriched in 10 KEEG pathways, no evidence of their involvement in metabolism pathways was identified and some of the bioinformatically enriched pathways, such as the PI3K-AKT and MAPK pathways, were experimentally excluded (Table S6; Figure 4i). Because the false negative effects of KEGG pathway enrichment can lead to a lack of significantly enrichment of metabolic pathways (Chen et al., 2017), we manually analyzed gene expressions related to glycolysis (Figure 6a), the tricarboxylic acid cycle (TCA) (Figure 6b), fatty acid oxidation (Figure 6c), and the pentose phosphate pathway (PPP) (Figure 6d). However, we failed to detect any TCA- or pentose phosphate pathway-related DEGs between the m.14487T- and m.14486C-containing cybrids (mean |FC| >1.5, $P_{adj} < 0.05$) (Figure 6b,d). Furthermore, gene expression related to glycolysis and fatty acid oxidation were barely affected since only a few DEGs (indicated by a dotted box in the Figure) (mean |FC| >1.5, $P_{adj} < 0.05$) were detected in some, but not all, of the mutant cybrids (Figure 6a,c). Taken together, our results suggest that the gene expression related to metabolic performance was minimally affected in cells carrying m.14487T>C mutations, when compared with control cells.
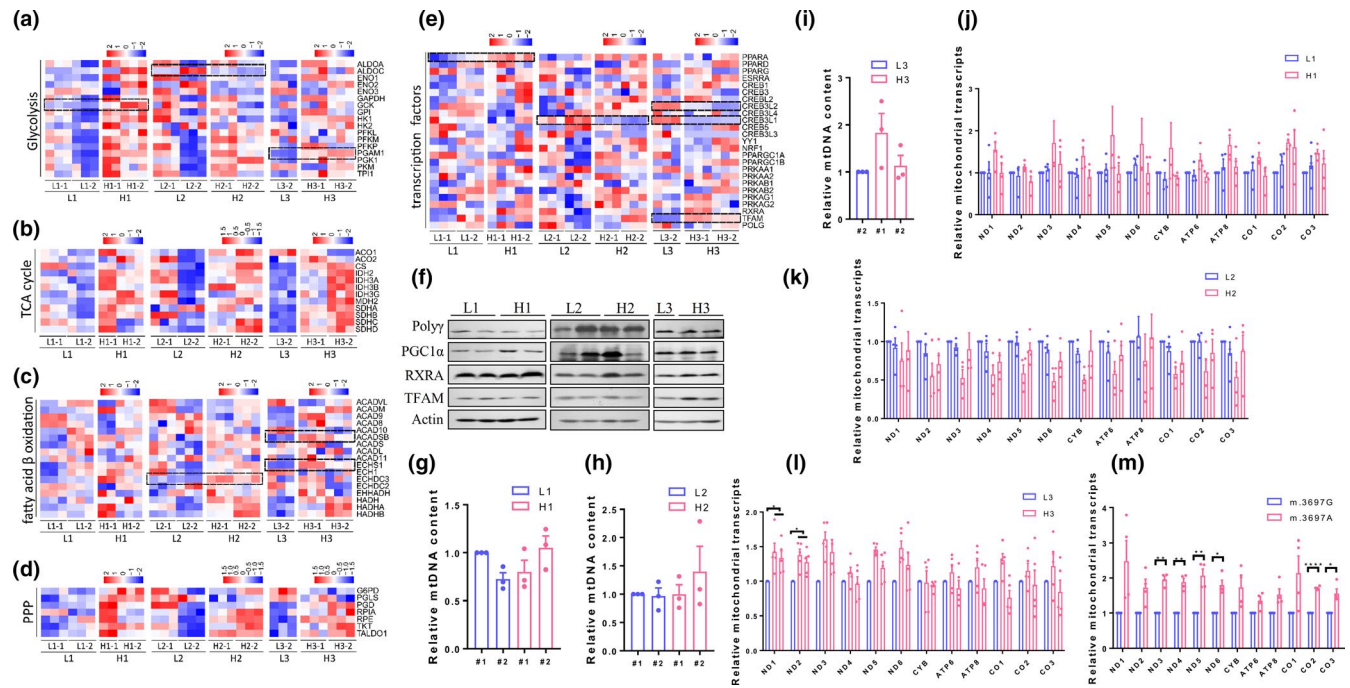
FIGURE 6 Transcriptome profiles were minimally affected by homoplasmic m.14487T>C mutations in cybrids cells. (a–d) Heatmap showing different gene expressions related to glycolysis (a), the tricarboxylic acid cycle (TCA) (b), fatty acid oxidation (c), and the pentose phosphate pathway (PPP) (d) in cybrids with or without m.14487T>C mutations ($n = 3$). Data were obtained by next-generation RNA sequencing of cybrids with or without m.14487T>C mutations. The gradual color change from red to blue represents the changing process from upregulation to downregulation. The genes with adjusted $p < .05$ and absolute fold change> 1.5 are indicated by a dotted box.(e) Heatmap showing different gene expressions of transcription factors related to mitochondrial function in cybrids with or without m.14487T>C mutations ($n = 3$). (f) Analysis of transcription factors related to mitochondrial function in cybrids with or without m.14487T>C mutations. Cell lysates were analyzed by western blot with antibodies against Polyγ, PGC1α, RXRA, and TFAM. Actin was used as the internal control. (g–i) Relative mtDNA content of cybrids containing m.14487T>C mutations from patient 1 (g), patient 2 (h), and patient 3 (i) and their paired control cybrids. (j–m) Relative mtRNA level of cybrids containing m.14487T>C mutations from patient 1 (j), patient 2 (k), and patient 3 (l) or m.3697G>A mutations (m) and their paired control cybrids. All experiments were performed independently at least thrice. Data are presented as means $\pm$ *SEM*. *$p < .05$, **$p < .01$, ***$p < .001$, ****$p < .0001$

Next, we analyzed the RNA levels of 25 transcription factors (Dominy & Puigserver, 2013), which may compensate for and restore mitochondrial function in cybrids with m.14487T>C mutations, but few of them were significantly affected by m.14487T>C mutation (as indicated by a dotted box in the Figure) (|FC| >1.5, $P_{adj} < 0.05$) (Figure 6e). Moreover, the protein analysis of four mitochondrial biogenesis-related transcription factors excluded the contribution of the patient 3-derived m.14487T>C mutation on mitochondrial transcription factor A (TFAM) levels (Figure 6f), and supported the notion that there is no compensatory boost of mitochondrial biogenesis in cybrids carrying m.14487T>C mutations (Figure 6f). Moreover, although mtDNA copy number was not affected (Figure 6g) and a slightly increase of mtRNA level was observed in patient 3-derived cybrids with m.14487T>C (Figure 6i), neither mtDNA copy number (Figure 6g–I) nor mtRNA level (Figure 6j–k) were significantly altered in cybrids carrying m.14487T>C mutations derived from patients 1 and 2, when compared with their paired control cybrids. Notably, a significantly increase of

mtRNA level was observed in cybrids with 3697G>A when compared with their paired control cells (Figure 6m). Taken together, our results suggest that the comparable mitochondrial OXPHOS function between m.14487T and m.14487C cybrids is not because of a compensatory boost of mitochondrial biogenesis in the m.14487C cybrids.

3.7 | Metabolic features were minimally affected by homoplasmic m.14487T>C mutations in cybrid cells

Changes in mitochondrial OXPHOS function are closely associated with metabolic reprogramming. Even a mild change in the OXPHOS within the normal range is sufficient to generate substantial changes in metabolites (Latorre-Pellicer et al., 2016). It is likely that metabolomics could be a sensitive and useful tool to evaluate possible changes in OXPHOS function. Therefore, we profiled metabolic features in cybrids with and without the given mtDNA mutations (m.14487T>C
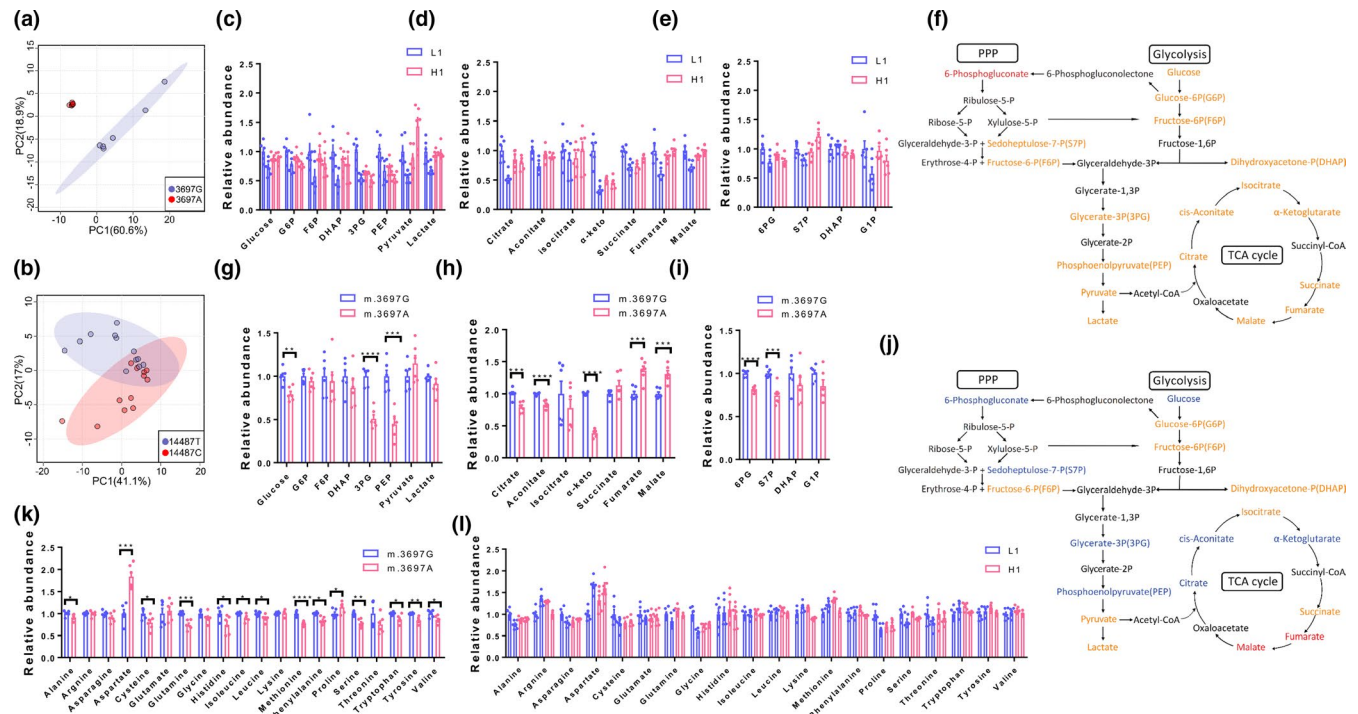
FIGURE 7 Metabolic features were minimally affected by homoplasmic m.14487T>C mutation in cybrids cells. (a–b) Principal component analysis (PCA) plot for samples with or without m.3697G>A mutations (a) ($n = 6$ per genotype) and samples with or without m.14487T>C mutations from patient 1 (b) ($n = 12$ per genotype). (c–e, l) Relative abundance of glycolysis (c), the tricarboxylic acid cycle (TCA) (d), the pentose phosphate pathway (PPP) (e) and amino acids (l) in cybrids containing m.14487T>C mutations from patient 1 and their paired control cybrids ($n = 12$). Data are normalized to the mean of the control cybrids. (f, j) Schematics of glycolysis, the TCA cycle, and the pentose phosphate pathway in cybrids with or without m.14487T>C mutations from patient 1 (f) or m.3697G>A mutations (j). Blue, red, yellow, and black mark metabolites which were downregulated, upregulated, unchanged, and unidentified, compared with control cybrids. (g–i, k) Relative abundance of glycolysis (g), the tricarboxylic acid cycle (TCA) (h), the pentose phosphate pathway (i) and amino acids (k) in cybrids containing m.3697G>A mutations and their paired control cybrids ($n = 6$). Data are normalized to the mean of the control cybrids. Data are presented as means $\pm$ SEM. **$p < .01$, ***$p < .001$, ****$p < .0001$

and m.3697G>A). Principal component analysis revealed a differential metabolic profile in cells with m.3697G>A when compared with control cells (Figure 7a), whereas the metabolic profiles of the cells with and without m.14487T>C mutation were shared (Figure 7b). This suggests that metabolic features may not be affected by m.14487T>C mutation. Furthermore, the metabolic pathways of glycolysis (Figure 7c), TCA (Figure 7d), and PPP (Figure 7e), which are tightly controlled by the OXPHOS, were barely affected by m.14487T>C mutation (Figure 7f). However, all three of these pathways were significantly altered in cells carrying m.3697G>A when compared with control cells (Figure 7g-j). Moreover, the levels of amino acids, including aspartate, glutamine, methionine, phenylalanine, serine, and tyrosine, were significantly affected by m.3697G>A mutation (Figure 7k), while none of these amino acids were affected by m.14487T>C mutation (Figure 7l). Notably, although decreased levels of aspartate have long been associated with OXPHOS deficiencies, both mass spectrometry and biochemistry-based aspartate determination supported the notion that aspartate was upregulated in cells with m.3697G>A when

compared with paired control cells (Figure 7l and Figure S4), indicating that the methods and experimental conditions we used in this study were reliable. Taken together, our results suggest that mitochondrial OXPHOS function was barely affected in cybrid cells carrying Chinese m.14487T>C mutations, and our metabolomic results suggest that m.14487T>C does not affect mitochondrial-associated metabolic features.

4 | DISCUSSION

In the past two decades, dozens of rare mtDNA mutations were identified as being associated with mitochondrial disease (Bannwarth et al., 2013). Unlike nDNA, mitochondrial diseases caused by heteroplasmic mtDNA mutations are clinically heterogeneous due to the heteroplasmic features of mtDNA at the molecular, cellular, tissue, and organ levels. For homoplasmic mtDNA mutations such as m.14484T>C and m.1555A>G, which have slight impacts on mitochondrial function, nuclear modifier genes including mitochondrial tRNA-specific 2-thiouridylase 1 (Guan et al., 2006) and

tyrosyl-tRNA synthetase 2 (Jiang et al., 2016) may be involved in causing varied clinical phenotypes in patients from the same pedigree. In this study, we confirmed that patient-derived lymphocytes with almost homoplasmic m.14487T>C mutations have decreased mitochondrial respiration and RCC I-related supercomplex assembly. However, it seems that homoplasmic m.14487T>C mutation has minimal effects on mitochondrial function in a transmitochondrial cybrid model. We believe that some currently unknown nuclear modifier genes may act synergistically with m.14487T>C to cause RCC I deficiency. Notably, m.14487T>C mutation has been functionally confirmed as a causative mutation for RCC I deficiency using similar transmitochondrial strategies as used in this study (Solano et al., 2003; Ugalde et al., 2003). Considering that the only difference between Ugalde et al.'s study model and ours is that they used a European-derived mtDNA genetic background (mtDNA haplogroup) and we used an East Asian one (Gonzalo et al., 2005; Solano et al., 2003; Ugalde et al., 2003), it is probable that mtDNA haplogroup may also contribute to the pathogenic role of m.14487T>C.

The pathogenic role of m.14487T>C in mitochondrial disease is very well accepted, and the mutation fulfills all criteria for it is pathogenicity (Gonzalez-Vioque, Bornstein, Gallardo, Fernandez-Moreno, & Garesse, 2014; Zaragoza, Brandon, Diegoli, Arbustini, & Wallace, 2011). Recently, the first preimplantation genetic diagnosis for m.14487T>C was performed for the birth of a clinically asymptomatic boy (Sallevelt et al., 2017). That is to say, any new conclusions related to the pathogenic role of m.14487T>C should be made very carefully. Transmitochondrial technology is frequently used to evaluate the contribution of mtDNA to OXPHOS function since noise from the nuclear genetic background is adjusted for (Schon, DiMauro, & Hirano, 2012; Wilkins, Carl, & Swerdlow, 2014) (Figure 1g). Using this model, both disease-causative mtDNA mutations and false positive mitochondrial disease-related mtDNA mutations were identified (Bornstein et al., 2002). In this study, we used transmitochondrial technology to test mitochondrial function in cybrids carrying m.14487T>C with additional cautions. An expanded number of cybrid clones and karyotyping were used to rule out potential nuclear influences in this study. Furthermore, we applied NGS to exclude private mutations during cybrid cell colonialization. Strikingly, two mtDNA mutations, m.3842G>A and m.11363G>A, were found in two cybrid cells derived from patient 3. Neither had been previously reported or maternally inherited. As neither of these mutations were detected via NGS sequencing of the blood of patient 3 or her mother, they were unlikely, although still possible, caused by a clonal expansion event during cybrid cell colonialization (Gorman et al., 2015; Greaves et al., 2014; Lakshmanan et al., 2018). It is possible that transmitochondrial procedures or cybrid cell colonialization may introduce a considerable number

of de novo mtDNA mutations. Although the mechanisms underlying the role of transmitochondrial technology in the derivation of de novo mutations need further investigation, mtDNA resequencing using NGS is recommended to exclude such mutations when making cybrid models. Biochemical evidence, such as decreased mitochondrial respiration, impaired OXPHOS enzymatic activity, or cells failing to grow in a galactose medium, are sufficient to claim a mitochondrial disorder in vitro. However, negative results in these biochemical indexes are not sufficient to exclude mitochondrial abnormality due to the possibility of compensatory effects on mitochondrial biogenesis (Liemburg-Apers, Schirris, Russel, Willems, & Koopman, 2015; Pacheu-Grau et al., 2018; Van Bergen et al., 2011). Mitochondrial to nuclear signaling plays a central role in the response to OXPHOS impairment (Chae et al., 2013). For example, increased mitochondrial ROS may be repressed by increasing the level of ROS-responsive NRF2, a master transcriptional regulator of antioxidant genes (Nguyen, Nioi, & Pickett, 2009). In addition, increased mitochondrial ROS and decreased ATP production may activate NRF1 and AMPK, respectively, to provide a compensatory boost to mitochondrial function via a transcriptional increase in the abundance of the mitochondrial master regulators, PPARGC1A alpha and PPAR-alpha (Liu & Butow, 2006). Therefore, it is necessary to exclude any possible compensatory responses due to mitochondrial damage in m.14487T>C cybrids. In this study, we examined mitochondrial to nuclear signaling at both the RNA and protein levels (Figures 4 and 5) and no mitochondria-related compensatory events were observed in the m.14487T>C cells. Transcriptional reprogramming related to metabolic pathways such as glycolysis can be achieved in cells with even minor changes in mitochondrial function (Picard et al., 2014); however, the transcriptional performance of the metabolic pathways did not differ between m.14487T and m.14487C cybrids, which was further confirmed by metabolome profiling. Since the threshold level for mitochondrial OXPHOS damage to induce transcriptome and metabolome reprogramming is unknown, we cannot identify to what degree OXPHOS function is being affected by m.14487T>C mutation. However, it is likely that transcriptional and metabolic reprogramming can be observed in cells with altered OXPHOS function before the appearance of biochemical evidence, such as the oxygen consumption index (Latorre-Pellicer et al., 2016; Picard et al., 2014).

In the theory of mitochondrial evolution medicine, mtDNA haplogroup plays an important role in the development of metabolic and degenerative disease (Fang et al., 2018; Wallace, 2005). Molecular epidemiology studies have shown that mtDNA haplogroup differently affects the clinical penetrance of LHON worldwide (Brown, Sun, & Wallace, 1997; Hudson et al., 2007; Wallace et al., 1988). A subsequent functional study revealed that mtDNA haplogroup differentially modulated the assembly kinetics of the OXPHOS

(Pello et al., 2008). In evolution, the characteristics of mtDNA can be shaped and influenced by nuclear genetic background in order to minimize the incompatibility of nDNA and mtDNA(Wei et al., 2019). And the individuals carrying mtDNA deleterious variant with mismatched nuclear–mtDNA genome are more likely to be pathological. This convincingly explains why m.14487T>C was functionally characterized as a damaging mutation in previous cybrid models but not in ours. However, further studies are needed to explore the contribution of other East Asian mtDNA haplogroups to m.14487T>C. While m.14487T>C mutation itself has a minimal effect on mitochondrial RCC I deficiency, unless in a combined patient nuclear genetic background, all the available evidence drives us to believe that nuclear modifier genes contribute to the pathogenicity of m.14487T>C. To identify secondary nDNA mutations related to m.14487T>C, we performed trio whole exome sequencing in family 2 and whole exome sequencing in an additional three patients, including patient 3. Unfortunately, we failed to detect any candidate mutations in the genes of RCC I or its assembled factors, following the published filtration strategy (Calvo et al., 2012). Thus, the identity of the nuclear modifier genes remains unknown.

In conclusion, we show that m.14487T>C with an East Asian mtDNA haplogroup has a minimal effect on mitochondrial function, and unknown nuclear modifier genes may be involved in regulating the pathogenicity of this mutation. Although further studies are needed to fully understand the role of m.14487T>C in mitochondrial disease, our findings partly clarify the underlying mechanisms by which the clinical features related to m.14487T>C display individual heterogeneity.

CONFLICT OF INTEREST

The authors report no conflicts of interest.

AUTHOR CONTRIBUTIONS
L.J., F.H., and Y.Y. planned the project and designed the experiments. Y.Y. collected samples. Z.Q., C.D, D.M., X.J., W.X., X.J., L.X., and H.Q. performed the biochemical experiments. C.D. and Z.H. performed the image experiments. W.X., X.J., and S.L. performed DNA studies. Z.Q. performed the transcriptome and metabolome studies. F.H. and Z.Q. wrote the manuscript. C.D., Z.Q., and L.T. revised the manuscript.

ORCID
Qiongya Zhao https://orcid.org/0000-0001-9616-4787
Jianxin Lyu https://orcid.org/0000-0003-2343-1666

REFERENCES

Alston, C. L., Heidler, J., Dibley, M. G., Kremer, L. S., Taylor, L. S., Fratter, C., … Taylor, R. W. (2018). Bi-allelic mutations in NDUFA6 establish its role in early-onset isolated mitochondrial complex I deficiency. *American Journal of Human Genetics*, *103*(4), 592–601. https://doi.org/10.1016/j.ajhg.2018.08.013

Balsa, E., Marco, R., Perales-Clemente, E., Szklarczyk, R., Calvo, E., Landazuri, M. O., & Enriquez, J. A. (2012). NDUFA4 is a subunit of complex IV of the mammalian electron transport chain. *Cell Metabolism*, *16*(3), 378–386. https://doi.org/10.1016/j.cmet.2012.07.015

Bannwarth, S., Procaccio, V., Lebre, A. S., Jardel, C., Chaussenot, A., Hoarau, C., … Paquis-Flucklinger, V. (2013). Prevalence of rare mitochondrial DNA mutations in mitochondrial disorders. *Journal of Medical Genetics*, *50*(10), 704–714. https://doi.org/10.1136/jmedgenet-2013-101604

Birch-Machin, M. A., & Turnbull, D. M. (2001). Assaying mitochondrial respiratory complex activity in mitochondria isolated from human cells and tissues. *Methods in Cell Biology*, *65*, 97–117.

Bornstein, B., Mas, J. A., Fernández-Moreno, M. A., Campos, Y., Martín, M. A., del Hoyo, P., … Garesse, R. (2002). The A8296G mtDNA mutation associated with several mitochondrial diseases does not cause mitochondrial dysfunction in cybrid cell lines. *Human Mutation*, *19*(3), 234–239. https://doi.org/10.1002/humu.10050

Brown, M. D., Sun, F., & Wallace, D. C. (1997). Clustering of Caucasian Leber hereditary optic neuropathy patients containing the 11778 or 14484 mutations on an mtDNA lineage. *American Journal of Human Genetics*, *60*(2), 381–387.

Calvo, S. E., Compton, A. G., Hershman, S. G., Lim, S. C., Lieber, D. S., Tucker, E. J., … Mootha, V. K. (2012). Molecular diagnosis of infantile mitochondrial disease with targeted next-generation sequencing. *Science Translational Medicine*, *4*(118), 118ra110. https://doi.org/10.1126/scitranslmed.3003310

Chae, S., Ahn, B. Y., Byun, K., Cho, Y. M., Yu, M.-H., Lee, B., … Park, K. S. (2013). A systems approach for decoding mitochondrial retrograde signaling pathways. *Science Signalling*, *6*(264), rs4. https://doi.org/10.1126/scisignal.2003266

Chen, L., Zhang, Y. H., Wang, S., Zhang, Y., Huang, T., & Cai, Y. D. (2017). Prediction and analysis of essential genes using the enrichments of gene ontology and KEGG pathways. *PLoS ONE*, *12*(9), e0184129. https://doi.org/10.1371/journal.pone.0184129

Chomyn, A., Lai, S. T., Shakeley, R., Bresolin, N., Scarlato, G., & Attardi, G. (1994). Platelet-mediated transformation of mtDNA-less human cells: Analysis of phenotypic variability among clones from normal individuals–and complementation behavior of the tRNALys mutation causing myoclonic epilepsy and ragged red fibers. *American Journal of Human Genetics*, *54*(6), 966–974.

Dermaut, B., Seneca, S., Dom, L., Smets, K., Ceulemans, L., Smet, J., … Santens, P. (2010). Progressive myoclonic epilepsy as an adult-onset manifestation of Leigh syndrome due to m.14487T>C. *Journal of Neurology, Neurosurgery and Psychiatry*, *81*(1), 90–93. https://doi.org/10.1136/jnnp.2008.157354

Dominy, J. E., & Puigserver, P. (2013). Mitochondrial biogenesis through activation of nuclear signaling proteins. *Cold Spring Harb Perspect Biol*, *5*(7), a015008–a015008. https://doi.org/10.1101/cshperspect.a015008

Eckenweiler, M., Catarino, C. B., Gallenmueller, C., Klopstock, T., Lagreze, W. A., Korinthenberg, R., & Kirschner, J. (2015).

Mitochondrial DNA mutation 14487T>C manifesting as Leber's hereditary optic neuropathy. *Journal of Neurology*, *262*(12), 2776–2779. https://doi.org/10.1007/s00415-015-7955-5

Fang, H., Hu, N., Zhao, Q., Wang, B., Zhou, H., Fu, Q., … Lyu, J. (2018). mtDNA haplogroup N9a increases the risk of type 2 diabetes by altering mitochondrial function and intracellular mitochondrial signals. *Diabetes*, *67*(7), 1441–1453. https://doi.org/10.2337/db17-0974

Fernandez-Vizarra, E., Ferrin, G., Perez-Martos, A., Fernandez-Silva, P., Zeviani, M., & Enriquez, J. A. (2010). Isolation of mitochondria for biogenetical studies: An update. *Mitochondrion*, *10*(3), 253–262. https://doi.org/10.1016/j.mito.2009.12.148

Fragouli, E., Spath, K., Alfarawati, S., Kaper, F., Craig, A., Michel, C.-E., … Wells, D. (2015). Altered levels of mitochondrial DNA are associated with female age, aneuploidy, and provide an independent measure of embryonic implantation potential. *PLoS Genetics*, *11*(6), e1005241. https://doi.org/10.1371/journal.pgen.1005241

Frazier, A. E., Thorburn, D. R., & Compton, A. G. (2017). Mitochondrial energy generation disorders: Genes, mechanisms and clues to pathology. *Journal of Biological Chemistry*, https://doi.org/10.1074/jbc.R117.809194

Frydrychova, R., & Marec, F. (2002). Repeated losses of TTAGG telomere repeats in evolution of beetles (Coleoptera). *Genetica*, *115*(2), 179–187.

Gaude, E., Schmidt, C., Gammage, P. A., Dugourd, A., Blacker, T., Chew, S. P., … Frezza, C. (2018). NADH shuttling couples cytosolic reductive carboxylation of glutamine with glycolysis in cells with mitochondrial dysfunction. *Molecular Cell*, *69*(4), 581–593 e587. https://doi.org/10.1016/j.molcel.2018.01.034

Gonzalez-Vioque, E., Bornstein, B., Gallardo, M. E., Fernandez-Moreno, M. A., & Garesse, R. (2014). The pathogenicity scoring system for mitochondrial tRNA mutations revisited. *Molecular Genetics & Genomic Medicine*, *2*(2), 107–114. https://doi.org/10.1002/mgg3.47

Gonzalo, R., Garcia-Arumi, E., Llige, D., Marti, R., Solano, A., Montoya, J., … Andreu, A. L. (2005). Free radicals-mediated damage in transmitochondrial cells harboring the T14487C mutation in the ND6 gene of mtDNA. *FEBS Letters*, *579*(30), 6909–6913. https://doi.org/10.1016/j.febslet.2005.11.034

Gorman, G. S., Pfeffer, G., Griffin, H., Blakely, E. L., Kurzawa-Akanbi, M., Gabriel, J., … Taylor, R. W. (2015). Clonal expansion of secondary mitochondrial DNA deletions associated with spinocerebellar ataxia type 28. *JAMA Neurol*, *72*(1), 106–111. https://doi.org/10.1001/jamaneurol.2014.1753

Greaves, L. C., Nooteboom, M., Elson, J. L., Tuppen, H. A. L., Taylor, G. A., Commane, D. M., … Turnbull, D. M. (2014). Clonal expansion of early to mid-life mitochondrial DNA point mutations drives mitochondrial dysfunction during human ageing. *PLoS Genetics*, *10*(9), e1004620. https://doi.org/10.1371/journal.pgen.1004620

Guan, M.-X., Yan, Q., Li, X., Bykhovskaya, Y., Gallo-Teran, J., Hajek, P., … Fischel-Ghodsian, N. (2006). Mutation in TRMU related to transfer RNA modification modulates the phenotypic expression of the deafness-associated mitochondrial 12S ribosomal RNA mutations. *American Journal of Human Genetics*, *79*(2), 291–302. https://doi.org/10.1086/506389

Hudson, G., Carelli, V., Spruijt, L., Gerards, M., Mowbray, C., Achilli, A., … Chinnery, P. F. (2007). Clinical expression of Leber hereditary optic neuropathy is affected by the mitochondrial DNA-haplogroup background. *American Journal of Human Genetics*, *81*(2), 228–233. https://doi.org/10.1086/519394

Ji, Y., Zhang, A. M., Jia, X., Zhang, Y. P., Xiao, X., Li, S., … Yao, Y. G. (2008). Mitochondrial DNA haplogroups M7b1'2 and M8a affect clinical expression of leber hereditary optic neuropathy in Chinese families with the m.11778G-->a mutation. *American Journal of Human Genetics*, *83*(6), 760–768. https://doi.org/10.1016/j.ajhg.2008.11.002

Jiang, P., Jin, X., Peng, Y., Wang, M., Liu, H., Liu, X., … Guan, M.-X. (2016). The exome sequencing identified the mutation in YARS2 encoding the mitochondrial tyrosyl-tRNA synthetase as a nuclear modifier for the phenotypic manifestation of Leber's hereditary optic neuropathy-associated mitochondrial DNA mutation. *Human Molecular Genetics*, *25*(3), 584–596. https://doi.org/10.1093/hmg/ddv498

Kirby, D. M., McFarland, R., Ohtake, A., Dunning, C., Ryan, M. T., Wilson, C., … Taylor, R. W. (2004). Mutations of the mitochondrial ND1 gene as a cause of MELAS. *Journal of Medical Genetics*, *41*(10), 784–789. https://doi.org/10.1136/jmg.2004.020537

Lakshmanan, L. N., Yee, Z., Ng, L. F., Gunawan, R., Halliwell, B., & Gruber, J. (2018). Clonal expansion of mitochondrial DNA deletions is a private mechanism of aging in long-lived animals. *Aging Cell*, *17*(5), e12814. https://doi.org/10.1111/acel.12814

Latorre-Pellicer, A., Moreno-Loshuertos, R., Lechuga-Vieco, A. V., Sánchez-Cabo, F., Torroja, C., Acín-Pérez, R., … Enríquez, J. A. (2016). Mitochondrial and nuclear DNA matching shapes metabolism and healthy ageing. *Nature*, *535*(7613), 561–565. https://doi.org/10.1038/nature18618

Lebon, S., Chol, M., Benit, P., Mugnier, C., Chretien, D., Giurgea, I., … Munnich, A. (2003). Recurrent de novo mitochondrial DNA mutations in respiratory chain deficiency. *Journal of Medical Genetics*, *40*(12), 896–899. https://doi.org/10.1136/jmg.40.12.896

Leshinsky-Silver, E., Shuvalov, R., Inbar, S., Cohen, S., Lev, D., & Lerman-Sagie, T. (2011). Juvenile Leigh syndrome, optic atrophy, ataxia, dystonia, and epilepsy due to T14487C mutation in the mtDNA-ND6 gene: A mitochondrial syndrome presenting from birth to adolescence. *Journal of Child Neurology*, *26*(4), 476–481. https://doi.org/10.1177/0883073810384615

Liemburg-Apers, D. C., Schirris, T. J., Russel, F. G., Willems, P. H., & Koopman, W. J. (2015). Mitoenergetic dysfunction triggers a rapid compensatory increase in steady-state glucose flux. *Biophysical Journal*, *109*(7), 1372–1386. https://doi.org/10.1016/j.bpj.2015.08.002

Liu, Z., & Butow, R. A. (2006). Mitochondrial retrograde signaling. *Annual Review of Genetics*, *40*, 159–185. https://doi.org/10.1146/annurev.genet.40.110405.090613

Malfatti, E., Bugiani, M., Invernizzi, F., de Souza, C.-F.-M., Farina, L., Carrara, F., … Zeviani, M. (2007). Novel mutations of ND genes in complex I deficiency associated with mitochondrial encephalopathy. *Brain*, *130*(Pt 7), 1894–1904. https://doi.org/10.1093/brain/awm114

Moehle, E. A., Shen, K., & Dillin, A. (2019). Mitochondrial proteostasis in the context of cellular and organismal health and aging. *Journal of Biological Chemistry*, *294*(14), 5396–5407. https://doi.org/10.1074/jbc.TM117.000893

Moreno-Lastres, D., Fontanesi, F., Garcia-Consuegra, I., Martin, M. A., Arenas, J., Barrientos, A., & Ugalde, C. (2012). Mitochondrial complex I plays an essential role in human respirasome assembly. *Cell Metabolism*, *15*(3), 324–335. https://doi.org/10.1016/j.cmet.2012.01.015

Negishi, Y., Hattori, A., Takeshita, E., Sakai, C., Ando, N., Ito, T., … Saitoh, S. (2014). Homoplasmy of a mitochondrial 3697G>A mutation causes Leigh syndrome. *Journal of Human Genetics*, *59*(7), 405–407. https://doi.org/10.1038/jhg.2014.41

Nguyen, T., Nioi, P., & Pickett, C. B. (2009). The Nrf2-antioxidant response element signaling pathway and its activation by oxidative stress. *Journal of Biological Chemistry*, *284*(20), 13291–13295. https://doi.org/10.1074/jbc.R900010200

Pacheu-Grau, D., Callegari, S., Emperador, S., Thompson, K., Aich, A., Topol, S. E., … Rehling, P. (2018). Mutations of the mitochondrial carrier translocase channel subunit TIM22 cause early-onset mitochondrial myopathy. *Human Molecular Genetics*, *27*(23), 4135–4144. https://doi.org/10.1093/hmg/ddy305

Pello, R., Martín, M. A., Carelli, V., Nijtmans, L. G., Achilli, A., Pala, M., … Ugalde, C. (2008). Mitochondrial DNA background modulates the assembly kinetics of OXPHOS complexes in a cellular model of mitochondrial disease. *Human Molecular Genetics*, *17*(24), 4001–4011. https://doi.org/10.1093/hmg/ddn303

Picard, M., Zhang, J., Hancock, S., Derbeneva, O., Golhar, R., Golik, P., … Wallace, D. C. (2014). Progressive increase in mtDNA 3243A>G heteroplasmy causes abrupt transcriptional reprogramming. *Proceedings of the National Academy of Sciences of the United States of America*, *111*(38), E4033–4042. https://doi.org/10.1073/pnas.1414028111

Qu, J., Zhou, X., Zhang, J., Zhao, F., Sun, Y. H., Tong, Y., Guan, M. X.. (2009). Extremely low penetrance of Leber's hereditary optic neuropathy in 8 Han Chinese families carrying the ND4 G11778A mutation. *Ophthalmology*, *116*(3), 558–564.e3. https://doi.org/10.1016/j.ophtha.2008.10.022

Rieder, M. J., Taylor, S. L., Tobe, V. O., & Nickerson, D. A. (1998). Automating the identification of DNA variations using quality-based fluorescence re-sequencing: Analysis of the human mitochondrial genome. *Nucleic Acids Research*, *26*(4), 967–973. https://doi.org/10.1093/nar/26.4.967

Sallevelt, S. C., Dreesen, J. C., Drusedau, M., Hellebrekers, D. M., Paulussen, A. D., Coonen, E., … de Die-Smulders, C. E. (2017). PGD for the m.14487 T>C mitochondrial DNA mutation resulted in the birth of a healthy boy. *Human Reproduction*, *32*(3), 698–703. https://doi.org/10.1093/humrep/dew356

Sambrook, J., & Russell, D. W. (2001). *Molecular cloning: A laboratory manual*. New York: Cold Spring Harbor Laboratory Press.

Schon, E. A., DiMauro, S., & Hirano, M. (2012). Human mitochondrial DNA: Roles of inherited and somatic mutations. *Nature Reviews Genetics*, *13*(12), 878–890. https://doi.org/10.1038/nrg3275

Signes, A., & Fernandez-Vizarra, E. (2018). Assembly of mammalian oxidative phosphorylation complexes I-V and supercomplexes. *Essays in Biochemistry*, *62*(3), 255–270. https://doi.org/10.1042/EBC20170098

Solano, A., Roig, M., Vives-Bauza, C., Hernandez-Peña, J., Garcia-Arumi, E., Playan, A., … Montoya, J. (2003). Bilateral striatal necrosis associated with a novel mutation in the mitochondrial ND6 gene. *Annals of Neurology*, *54*(4), 527–530. https://doi.org/10.1002/ana.10682

Sun, D., Li, B., Qiu, R., Fang, H., & Lyu, J. (2016). Cell type-specific modulation of respiratory chain supercomplex organization. *International Journal of Molecular Sciences*, *17*(6), https://doi.org/10.3390/ijms17060926

Ugalde, C., Triepels, R. H., Coenen, M. J. H., Van Den Heuvel, L. P., Smeets, R., Uusimaa, J., … Nijtmans, L. G. J. (2003). Impaired complex I assembly in a Leigh syndrome patient with a novel missense mutation in the ND6 gene. *Annals of Neurology*, *54*(5), 665–669. https://doi.org/10.1002/ana.10734

Van Bergen, N. J., Crowston, J. G., Kearns, L. S., Staffieri, S. E., Hewitt, A. W., Cohn, A. C., … Trounce, I. A. (2011). Mitochondrial oxidative phosphorylation compensation may preserve vision in patients with OPA1-linked autosomal dominant optic atrophy. *PLoS ONE*, *6*(6), e21347. https://doi.org/10.1371/journal.pone.0021347

Wallace, D. C. (2005). A mitochondrial paradigm of metabolic and degenerative diseases, aging, and cancer: A dawn for evolutionary medicine. *Annual Review of Genetics*, *39*, 359–407. https://doi.org/10.1146/annurev.genet.39.110304.095751

Wallace, D. C., Singh, G., Lott, M. T., Hodge, J. A., Schurr, T. G., Lezza, A. M., … Nikoskelainen, E. K. (1988). Mitochondrial DNA mutation associated with Leber's hereditary optic neuropathy. *Science*, *242*(4884), 1427–1430.

Wang, J., Brautbar, A., Chan, A. K., Dzwiniel, T., Li, F. Y., Waters, P. J., … Wong, L. J. (2009). Two mtDNA mutations 14487T>C (M63V, ND6) and 12297T>C (tRNA Leu) in a Leigh syndrome family. *Molecular Genetics and Metabolism*, *96*(2), 59–65. https://doi.org/10.1016/j.ymgme.2008.10.006

Wang, Y., Wu, F., Pan, H., Zheng, W., Feng, C., Wang, Y., … Chen, S. (2016). Lost region in amyloid precursor protein (APP) through TALEN-mediated genome editing alters mitochondrial morphology. *Scientific Reports*, *6*, 22244. https://doi.org/10.1038/srep22244

Wei, W., Tuna, S., Keogh, M. J., Smith, K. R., Aitman, T. J., Beales, P. L., … Chinnery, P. F. (2019). Germline selection shapes human mitochondrial DNA diversity. *Science*, *364*(6442), https://doi.org/10.1126/science.aau6520

Wilkins, H. M., Carl, S. M., & Swerdlow, R. H. (2014). Cytoplasmic hybrid (cybrid) cell lines as a practical model for mitochondriopathies. *Redox Biology*, *2*, 619–631. https://doi.org/10.1016/j.redox.2014.03.006

Wittig, I., Braun, H. P., & Schagger, H. (2006). Blue native PAGE. *Nature Protocols*, *1*(1), 418–428. https://doi.org/10.1038/nprot.2006.62

Zaragoza, M. V., Brandon, M. C., Diegoli, M., Arbustini, E., & Wallace, D. C. (2011). Mitochondrial cardiomyopathies: How to identify candidate pathogenic mutations by mitochondrial DNA sequencing, MITOMASTER and phylogeny. *European Journal of Human Genetics*, *19*(2), 200–207. https://doi.org/10.1038/ejhg.2010.169

Zhou, C., Sun, H., Zheng, C., Gao, J., Fu, Q., Hu, N., … Lyu, J. (2018). Oncogenic HSP60 regulates mitochondrial oxidative phosphorylation to support Erk1/2 activation during pancreatic cancer cell growth. *Cell Death & Disease*, *9*(2), 161. https://doi.org/10.1038/s41419-017-0196-z

Zinchuk, V., Wu, Y., & Grossenbacher-Zinchuk, O. (2013). Bridging the gap between qualitative and quantitative colocalization results in fluorescence microscopy studies. *Scientific Reports*, *3*, 1365. https://doi.org/10.1038/srep01365

SUPPORTING INFORMATION

Additional supporting information may be found online in the Supporting Information section.